2024 IEEE International Conference on Microwaves, Communications, Antennas, Biomedical Engineering and Electronic Systems (COMCAS)

2024 IEEE International Conference on Microwaves, Communications, Antennas, Biomedical Engineering and Electronic Systems (COMCAS) | 979-8-3503-4818-7/24/$31.00 ©2024 IEEE | DOI: 10.1109/COMCAS58210.2024.10666190

Sliding Metagratings for Dynamic Beam Switching Via Rigorous Floquet-Bloch Theory

Sherman W. Marcus and Ariel Epstein
Andrew and Erna Viterbi Faculty
of Electrical and Computer Engineering
Technion – Israel Institute of Technology
Haifa 3200003, Israel
shermanm@technion.ac.il

***Abstract*—Wire-based metagratings, consisting of parallel arrays of periodic capacitively loaded wires which can be etched onto printed circuit boards (PCBs), have been shown capable of efficient control of waves. In particular, they can suppress Floquet-Bloch (FB) modes in undesired directions, thereby concentrating the energy of a beam in a given FB direction of interest. A method is presented herein to vary this beam direction by sliding the PCBs (and their resident wire arrays) to new locations, thereby providing a low-loss method of beam switching. The locations and distributed capacitive reactances of these wire arrays are determined by applying straightforward optimization techniques to a rigorous FB mathematical model. The efficiency of these beam switching solutions, verified using full-wave methods, are shown to exceed 90% for all designated radiation states.**

***Index Terms*—metagratings, Floquet-Bloch modes, beam-switching**

I. Introduction

Metagratings (MGs) have been shown capable of efficiently controlling the directions of reflected and refracted waves [1], relying on sparse constellations of polarizable particles (meta-atoms) judiciously positioned and shaped. By tailoring the mutual interactions between the individual scatterers, a desired interference pattern can be obtained [1]–[3], often with performance figures superseding those of dense metasurface counterparts [4], [5]. An appealing loaded-wire MG configuration compatible with standard printed-circuit-board (PCB) formations has been proposed recently, utilizing a rigorous analytical model to devise and experimentally demonstrate effective wave control at microwave frequencies [3], [6]–[10].

Dynamic control of a reflected or refracted beam with metasurfaces and metagratings has been traditionally achieved at microwave frequencies by employing non-linear components (diodes) [11]–[14]; alas, such components usually suffer from non-negligible losses, which become more severe as the operating frequency increases. As a possible alternative, we have recently proposed a low-loss solution for dynamic beam switching, by controlling the space between a periodic surface and multi-modal anti-reflective coatings (MMARC) [15], [16], relying on electronically controlled mechanical motion for reconfigurability [17]. However, switching between more than two directions has been found to be particularly challenging, and the methodology was limited to reflection mode operation. Herein, we address these challenges, and demonstrate that more involved transmissive beam-switching can be achieved by a system of MGs which slide relative to each other, each consisting of a PCB etched with capacitively-loaded wire strips (Fig. 1). Harnessing rigorous Floquet-Bloch (FB) theory to analyze multiple lateral shifting and capacitive load configurations, a multifunctional opmization problem is formulated, based on the high-fidelity analytical model governing MG synthesis. Consequently, the required meta-atom (loaded-wire) coordinates and geometries of the switched-beam device can be found, including the sliding distances associated with each radiation state. The resultant fabrication-ready design, avoiding full-wave optimizations in commercial solvers, may provide a low-loss solution to beam switching and other future wave control applications.

II. Theory

Consider a stack of PCBs on which periodic arrays of capacitively-loaded wires are etched (Fig. 1), and which is illuminated by a transverse electric (TE) incident wave. The electric field in each layer m of this stack can be expressed as a sum of discrete Floquet-Bloch (FB) modes [3], [6], [8], [18],

$$\mathbf{E}^{(m)}(x,y) = \sum_{p=-\infty}^{\infty} e^{ik_{xp}x} E_p^{(m)}(y)\hat{\mathbf{z}}, \tag{1}$$

where k_{xp} is the transverse component of the wave number for mode p, the configuration is invariant in the z-direction, periodic in the x-direction, and an $e^{-i\omega t}$ time dependence is suppressed. The interaction of these modal fields with the capacitively-loaded wires induces currents in them which, in accordance with Ohm's law, are influenced by the capacitive loading [3], [18]. In this sense, the distributed capacitance of the wire acts as a degree-of-freedom in the problem. The wire-field interaction serves to couple the modes one to another, and is fully considered in our formulation which follows [8]. By satisfying tangential field continuity conditions at boundaries between different materials (e.g. between the PCB dielectric and air), and discontinuity of the tangential magnetic field across wire arrays, we solve for the unknown FB-mode amplitudes $E_p^{(m)}$ in each dielectric layer. Although this formulation fully includes evanescent wave components,

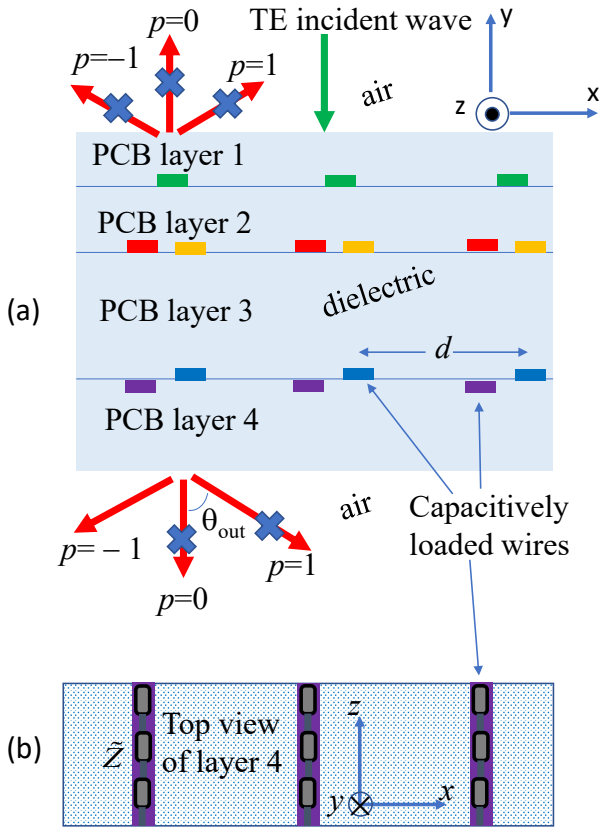

Fig. 1. (a) Parallel arrays of periodic capacitively loaded wires affixed to PCBs. The configuration is illuminated from above by a normally incident TE wave (green arrow) which is scattered reflectively and transmissively into a discrete spectrum of Floquet-Bloch (FB) waves, the propagating components of which are indicated by red arrows. Our formulation is meant to minimize all of these propagating FB components except the one of interest. In the figure, the FB component of interest is the transmissive $p = -1$ mode. PCB layers 1 and 3 are each etched with a single wire array at the bottom of the layer. PCB layer 2 is etched with two wire arrays. PCB layer 4 is etched with a single wire array at the top of the layer. For reasons of symmetry, the beam switching is compatible with only a single wire array per PCB layer, precluding the configuration of PCB layer 2. Although not mandatory, the PCB layers will be placed "back-to-back" as illustrated for PCB layer 3 relative to PCB layer 4. Note that whereas the wires are in reality etched *onto* the PCB, they are illustrated as etched *into* the PCB to emphasize the linkage of the PCB with the wire array. The wires are sufficiently thin that the array of layer 3 can be considered as colinear with the array of layer 4. (b) The top view of PCB layer 4, displaying the distributed capacitive reactance $\tilde{Z}$ of its wires. Although illustrated as short discrete capacitors, the wire is modeled as having a continuous, distributed capacitance per unit length along the wire.

in the outer (free space) regions we are principally interested in the propagating wave components (red arrows in Fig. 1) since only these radiate energy. For the case of normal TE incidence and refraction to $\theta_{\text{out}} > 30°$, for instance (Fig. 1), there is a total of six propagating waves: three upward (reflected) waves in the $-\theta_{\text{out}}$, $0°$ and $+\theta_{\text{out}}$ directions, and three downward (transmitted) waves in the $-\theta_{\text{out}}$, $0°$ and $+\theta_{\text{out}}$ directions. These correspond to modes $p = -1$, $p = 0$ and $p = 1$ in (1). Therefore, as shown schematically in Fig. 1, if we are interested in producing a transmitted beam in the $-\theta_{\text{out}}$ direction, we must find the metagrating configuration that minimizes the amplitudes of the five waves in the other propagating directions, allowing all the energy to propagate in the desired transmissive $-\theta_{\text{out}}$ direction [8].

We apply the *lsqnonlin* Matlab non-linear optimization function to our mathematical model to find the metagrating configuration which minimizes all these propagating wave components except the one we are interested in. The degrees of freedom at our disposal for finding such a configuration are (i) the lateral location of each wire array, such as the blue wires of layer 3 and the purple wires of layer 4 in Fig. 1(a); and (ii) the distributed capacitive reactance of the wires in each array, such as the purple wires of layer 4 in Figs. 1(a) and 1(b).

A parameter that we have defined *a priori* is the number of wire arrays that we employ. In [8], four wire arrays were required to control four propagating FB modes. It is therefore reasonable to assume in our case, where there are six propagating waves to be controlled, that six wire arrays should be employed. This is indeed what was done. However, whereas in [8] multiple arrays were employed on a single PCB facet, it is advantageous for our beam-switching application to limit ourselves to a single wire array per PCB. As stated in Section I, our goal is to vary the direction of the refracted wave by sliding the wire-array-etched PCBs relative to each other (i.e., varying the lateral location of the wire arrays). This change in configuration of the metagratings is designed to change the FB component that is maximized as in Fig. 1. Since we are assuming normal incidence to the surface ($\theta_{\text{in}} = 0°$), if a metagrating configuration is found that refracts the beam to the $-\theta_{\text{out}}$ direction, a symmetrical configuration would refract the beam to the $+\theta_{\text{out}}$ direction. Such a symmetrical configuration cannot generally be formed by our sliding procedure unless the location of each individual wire array can be controlled, thus precluding the possibility of multiple arrays on a single PCB.

Based on the above, if each PCB contains only a single wire array, then if a solution is found for the beam in the $-\theta_{\text{out}}$ direction, it is possible to laterally slide the PCBs to symmetric locations to produce a beam in the $+\theta_{\text{out}}$ direction. But the requirements in our case are more demanding. Not only do we wish to find the wire array locations and distributed capacitive reactances which provide efficient refraction to the $-\theta_{\text{out}}$ direction, but we would also like to find *different* lateral locations for the *same* wire arrays to provide refraction to the $0°$ direction. Use of the same wire arrays implies use of the same capacitive reactances. These capacitive reactances will therefore not represent degrees of freedom for optimizing the coupling to the $0°$ direction.

III. Results and Discussion

To verify our theoretical framework, we will consider wires of width 4 mil etched onto Rogers 3003 substrates 30 mil thick [19] characterized by relative permittivity 3 and $\tan\delta = 0.001$. The frequency is 20 GHz and the refraction angle is chosen to be $\theta_{\text{out}} = 60°$, so that the period d of our device is

$$d = \frac{\lambda}{|\sin\theta_{\text{out}} - \sin\theta_{\text{in}}|} = 1.154\lambda. \tag{2}$$

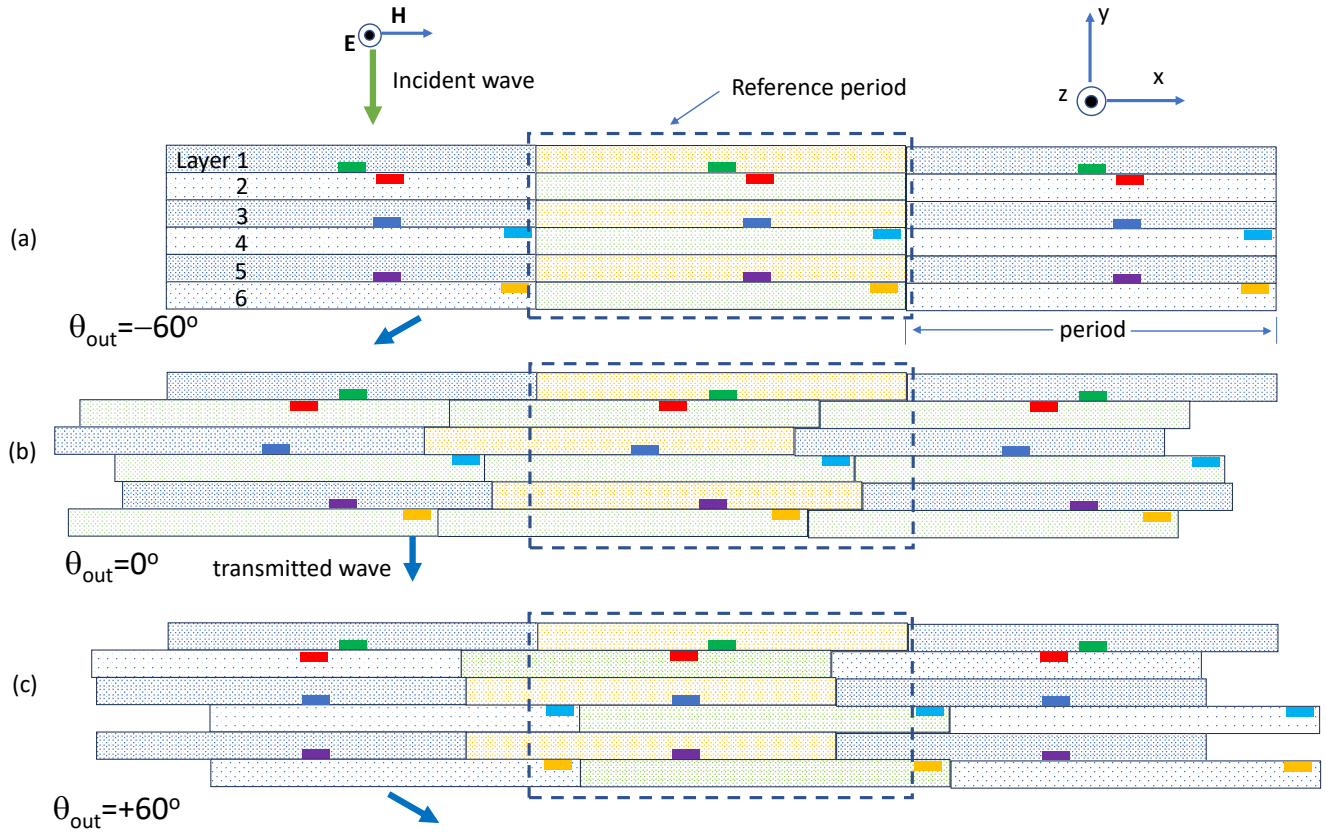

Fig. 2. Sliding metagratings capable of producing beams in different directions in accordance with the lateral location of each metagrating relative to a reference period (dashed box). Three complete periods of each layer are shown. Each metagrating consists of a dielectric layer (PCB) 0.0505λ thick, dielectric constant 3, loss tangent 0.001, with a single thin wire strip etched onto it per period along the x-direction. The green, red, blue, cyan, purple and orange strips are etched onto PCB layers 1, 2, 3, 4, 5 and 6, respectively, and the required distributed load impedances were found to be $\tilde{Z} = i[3.30, 9.91, 4.44, 4.66, 9.79, 4.77]\eta/\lambda$, where η is the free space impedance. Although the layer thicknesses are drawn to scale relative to the period, the wire strips are drawn larger-than-scale in order to improve their visibility; they are actually much thinner and narrower than shown in the figure. The configurations produce transmitted beams in the directions of the bold blue arrows: (a) $-60°$, (b) $0°$ and (c) $60°$.

where λ is the wavelength. We follow the prescribed methodology outlined in Section II by truncating the infinite sum in (1) to 21 modes (in air: 3 propagating modes and 18 evanescent modes). This will provide optimized analytical solutions for which the refracted beam direction can be switched from one direction to another by sliding the PCBs from one lateral configuration to another. Without any further optimization, we will transfer our analytic solution to a full-wave simulator (CST) [20], and compare the scattered fields to the ones anticipated by our analytical model.

Fig. 2 illustrates the wire array locations, and lists their distributed capacitive reactances, that were determined by our analytical model to produce beams in the FB directions of Fig. 1. The configurations of Figs. 2(a), 2(b) and 2(c) produce the analytical electric fields shown in Figs. 3(a), 3(b) and 3(c), respectively, as determined by our mathematical model. Each configuration can be formed from any of the other configurations by sliding five of the six PCBs to the proper location; since the influence on the field is determined by the *relative* location of each wire array, one of the arrays can remain fixed in place. In Fig. 2, this fixed array was chosen to be the topmost (green) array. It is then possible to divide that topmost layer into period-long segments, so that the "green" wire is in the center of such a segment. This defines the "reference period" shown in Fig. 2. In fact, defining the configuration of Fig. 2(a) as the "reference configuration", it is possible to choose the period-long segments of the other five layers to coincide with the lateral location of the "reference period". This defines the dashed box which, for the reference configuration Fig. 2(a), contains a single period-long segment from each of the layers. This reference period box will now be used to clarify the extent that the PCB layers are slid to produce beams in the other directions.

As stated, the PCB/wire configuration of Fig. 2(a) was found by our analytical model to produce the refracted field shown in Fig. 3(a); i.e., a beam in the $-60°$ direction. To switch to the

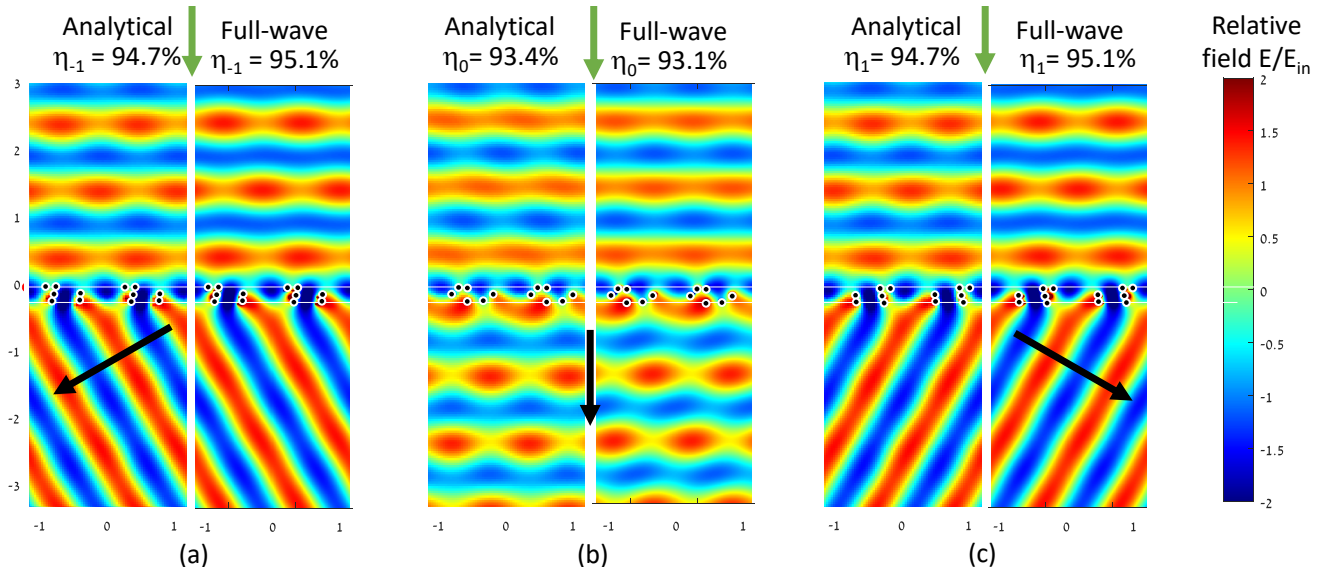

Fig. 3. Two periods of the E-field as predicted by our analytical method and verified by full-wave CST calculations for the metagrating structures shown in (a) Fig. 2(a) for producing a refracted wave in the -60° direction; (b) Fig. 2(b) for producing a refracted wave in the 0° direction; and (c) Fig. 2(c) for producing a refracted wave in the $+60^\circ$ direction. These metagrating structures are located between the respective white horizontal lines in each of the figures, with the wires shown as black dots. The axes are scaled to units of λ. The coupling efficiencies η_{-1}, η_0 and η_1 for propagating modes -1, 0 and $+1$, respectively, exceed 93% for each case.

beam shown in Fig. 3(b) in the 0° direction, it is necessary to slide the PCB layers in Fig. 2(a) to the analytically-determined configuration in Fig. 2(b). From the period-segment positions in the dashed reference period box of Fig. 2(b), it is seen that [coincidentally] all five of the movable layers had to be slid different amounts to the left. Because of periodicity, no layer need be slid a distance greater than $d/2$; if a movement of more than $d/2$ is required in one direction, the same relative location of the array can be achieved by a movement less than $d/2$ in the other direction.

Although the metagrating solutions of Figs. 2(a) and 2(b) were obtained with the aid of the nonlinear equation solver, the configuration in Fig. 2(c), which produces the refraction shown in Fig. 3(c) in the $+60^\circ$ direction, was obtained simply as the mirror image of the wires of Fig. 2(a). This was possible since $\theta_{\text{in}} = 0^\circ$. Indeed, we chose normal incidence precisely to facilitate solution of this part of the problem based on symmetry. As may be seen in Fig. 2(c), the symmetry with respect to Fig. 2(a) is relative to the center of the topmost (green) wire. The configuration of Fig. 2(c) may be reached from that of Fig. 2(a) by sliding layers 2, 3 and 5 the specified amounts to the left, and sliding layers 4 and 6 the specified amounts to the right. Again, all movements were computed by our analytical model, and involve distances less than $d/2$.

The analytical results of Fig. 3, obtained from our mathematical model, confirm the beam-switching functionality of utilizing a single passive PCB stack with sliding mechanism to deflect the incoming wave with high ($> 93\%$) coupling efficiency. To verify the performance of the designed device, the same PEC-wired stack configurations were defined and simulated in CST Microwave studio [20] without any further optimization. The resulting full-wave fields are shown in Fig. 3 as well. As clearly observed, excellent agreement is obtained between analytical predictions and full-wave simulations, demonstrating the validity of our mathematical model. The coupling efficiencies computed by our analytical model (and by CST) are $\eta_{-1} = 94.7\%(95.1\%)$, $\eta_0 = 93.4\%(93.1\%)$ and $\eta_1 = 94.7\%(95.1\%)$. In CST, the substitution of copper for PEC leads to a 1/2% degradation in η_0, and a degradation of 5 percentage points in η_{-1} and η_1. The resulting coupling efficiencies remain above 90%, even in the presence of such realistic conductor loss.

IV. Conclusion

We have proposed and numerically implemented a low-loss method for dynamic beam switching by simply sliding each layer of a stack of metagratings to new relative positions. The layers of this stack are defined by an analytical model, without the need for full-wave optimization. The results of the analytical model have been validated by full-wave calculations. For the 60° refraction considered here, the efficiency of these beams has been shown to exceed 90% (taking conductor and dielectric losses into account). Future work will include smaller refraction angles and a consequently greater number of beam directions.

It is envisioned that the conceptual simplicity of this method, combined with its high coupling efficiencies, will make it a serious candidate for beam switching and other future wave control applications.

Acknowledgment

This work was supported by the Israel Innovation Authority through its Metamaterials Consortium.

REFERENCES

[1] Y. Ra'di and A. Alù, "Metagratings for efficient wavefront manipulation," *IEEE Photonics Journal*, vol. 14, 2022.

[2] Y. Ra'di, D. L. Sounas, and A. Alù, "Metagratings: Beyond the limits of graded metasurfaces for wave front control," *Phys. Rev. Lett.*, vol. 119, p. 067404, 2017.

[3] A. Epstein and O. Rabinovich, "Unveiling the properties of metagratings via a detailed analytical model for synthesis and analysis," *Phys. Rev. Appl.*, vol. 8, p. 054037, 2017.

[4] M. Chen, E. Abdo-Sánchez, A. Epstein, and G. Eleftheriades, "Theory, design, and experimental verification of a reflectionless bianisotropic huygens' metasurface for wide-angle refraction," *Phys. Rev. B*, vol. 97, p. 125433, 2018.

[5] G. Lavigne, K. Achouri, V. Asadchy, S. Tretyakov, and C. Coloz, "Susceptibility derivation and experimental demonstration of refracting metasurfaces without spurious diffraction," *IEEE Trans. Antennas Propag.*, vol. 66, p. 1321–1330, 2018.

[6] O. Rabinovich and A. Epstein, "Analytical design of printed circuit board (pcb) metagratings for perfect anomalous reflection," *IEEE Trans. Antennas Propag.*, vol. 66, pp. 4086–4095, 2018.

[7] V. Popov, F. Boust, and S. Burokur, "Controlling diffraction patterns with metagratings," *Phys. Rev. Applied*, vol. 10, p. 011002, 2018.

[8] O. Rabinovich and A. Epstein, "Arbitrary diffraction engineering with multilayered multielement metagratings," *IEEE Trans. Antennas Propag.*, vol. 68, pp. 1553–1568, 2020.

[9] G. Xu, S. Hum, and G. Eleftheriades, "Dual-band reflective metagratings with interleaved meta-wires," *IEEE Trans. Antennas Propag.*, vol. 69, p. 2181–2193, 2021.

[10] G. Xu, G. Eleftheriades, and S. Hum, "Analysis and design of general printed circuit board metagratings with an equivalent circuit model approach," *IEEE Trans. Antennas Propag.*, vol. 69, p. 4657–4669, 2021.

[11] S. Hum and J. Perruiseau-Carrier, "Reconfigurable reflectarrays and array lenses for dynamic antenna beam control: a review," *IEEE Trans. Antennas Propag.*, vol. 62, pp. 183–198, 2014.

[12] Tian, H. and Memarian, M. and Itoh, T., "Electronically-tunable resonant blazed metasurface grating," *2017 IEEE Asia Pacific Microwave Conference (APMC)*, p. 376–379, 2017.

[13] A. Casolaro, A. Toscano, A. Alu, and F. Bilotti, "Dynamic beam steering with reconfigurable metagratings," *IEEE Trans. Antennas Propag.*, vol. 68, p. 1542–1552, 2020.

[14] V. Popov, B. Ratni, S.N. Burokur and F. Boust, "Non-local reconfigurable sparse metasurface: efficient near-field and far-field wavefront manipulations," *Adv. Optical Mater.*, vol. 9, p. 2001316, 2021.

[15] S.W. Marcus and A. Epstein, "Dynamic beam switching with shiftable multimodal anti-reflective coatings," in *2021 IEEE International Conference on Microwaves, Antennas, Communications and Electronic Systems (COMCAS)*, pp. 508–512, 2021.

[16] S. Marcus, V. Killamsetty, Y. Yashno, and A. Epstein, "Multimodal antireflective coatings for perfecting anomalous reflection from arbitrary periodic structures," *Phys. Rev. B*, vol. 106, p. 205132, 2022.

[17] M. Mavridou and A.P. Feresidis, "Dynamically reconfigurable high impedance and frequency selective metasurfaces using piezoelectric actuators," *IEEE Trans. Antennas Propag.*, vol. 12, pp. 5190–5197, 2016.

[18] S. Tretyakov, *Analytical modeling in applied electromagnetics*. Artech House, 2003.

[19] https://www.rogerscorp.com/-/media/project/rogerscorp/documents/advanced-connectivity-solutions/english/data-sheets/ro3000-laminate-data-sheet-ro3003—-ro3006—-ro3010—-ro3035.pdf.

[20] https://www.3ds.com/products-services/simulia/products/cst-studio-suite/.